Bulletin of the Seismological Society of America, Vol. 93, No. 1, pp. 203–214, February 2003

Moment Magnitude Determination for Local and Regional Earthquakes Based on Source Spectra

by Lars Ottemöller* and Jens Havskov

Abstract We investigated the use of an automated routine to determine moment magnitudes from the displacement spectra of local and regional earthquakes. Two algorithms, a genetic algorithm and a converging grid search, were developed and tested with earthquake data from Mexico, Norway, and Deception Island (Antarctica). It was found that compared with manual analysis, the algorithms give reliable automatic moment magnitude (M_w) estimates in the range $-1 < M < 8$. The converging grid search appeared to be more cost-effective than the genetic algorithm. M_w at local and regional distances seems superior to amplitude-based magnitudes that saturate for large earthquakes. The application of the automated algorithm in near real time may help to obtain a nonsaturated magnitude estimate in the case of a large earthquake immediately after the earthquake has occurred. Also, the method can be useful for processing large amounts of data.

Introduction

Earthquakes can be quantified in terms of energy release, which is related to the fault dimensions, slip, and stress drop. The actual ground movement at a given location depends on the radiation pattern, propagation along the travel path, and local site conditions. Averaging over the effects of geometric spreading and attenuation, the magnitude concept was developed to quantify the size of earthquakes (Kanamori, 1983). Most magnitude scales in use, such as M_L, M_B, and M_S, are based on the measurement of time-domain amplitudes on the seismograms. Also, the M_c scale, which is based on the signal duration, is widely used at local distances. Alternatively, magnitude determination based on frequency-domain measurements has been investigated (e.g., Grant and Mansinha, 1977; Nortmann and Duda, 1983). The moment magnitude scale (M_w) as defined by Kanamori (1977) has the advantage of not saturating for the largest earthquakes, unlike the amplitude-based scales (e.g., Hanks and Kanamori, 1979). Most seismologists agree that M_w, which is based on a physical quantity, the seismic moment, and is nonsaturating for great earthquakes, should be the prime magnitude scale. However, the more traditional amplitude-based scales are still more common and at least provide historic continuity (Miyamura, 1982).

Throughout the world, a large and growing number of local and regional seismic networks are operated in near real time to facilitate fast response in the case of destructive earthquakes (Espinosa Aranda *et al.*, 1995; Johnson *et al.*, 1995; Gee *et al.*, 1996; Malone, 1996; Wu *et al.*, 1997). The main objective of the near real-time operation is to determine the earthquake location, depth, and size as fast as possible. This process involves automatic phase identification (e.g., Withers *et al.*, 1998) and hypocenter determination. The earthquake size in most automatic systems is determined by time domain amplitude measurements or the signal duration. Systems for automatic determination of source parameters including the seismic moment have been developed by McEvilly and Majer (1982), Anderson and Humphrey (1991), Schindelé *et al.* (1995), and Al-Eqabi *et al.* (2001). Automatic routines for source-parameter determination make it feasible to analyze large data sets and at the same time are considered to be more objective (Anderson and Humphrey, 1991). Alternatively, the seismic moment is routinely obtained from regional broadband recordings through automated moment tensor inversion (Kawakatsu, 1995; Pasyanos *et al.*, 1996). Even the feasibility of a real-time waveform inversion for moment tensor and centroid location has been investigated (Tajima *et al.*, 2002).

In recent destructive earthquakes it has been seen that the first-magnitude estimates from local and regional networks can be off by more than one order. For example after the Kocaeli, Turkey, M_w 7.4 earthquake of 17 August 1999 (Toksöz *et al.*, 1999), the first magnitude reported was M_c 6.7 (Kandilli Observatory). After the Kachchh, India, M_w 8.0 earthquake of 26 January 2001 (Gupta et al., 2001) the local seismic network (India Meteorological Department) reported M_L 6.9. The El Salvador M_w 7.7 earthquake of 13 January 2001 (Lomnitz and Eliarrarás, 2001) was initially reported with magnitudes of M_c 6.0 and M_L 6.8 by the regional Central American Seismic Center (CASC). In these

*Present address: British Geological Survey, Edinburgh, U.K.

examples the underestimation of magnitude is due to saturation of the magnitude scales applied. The underestimation due to saturated scales (M_L and M_B) can lead to fatal misjudgement of the situation. However, for these examples it is unclear what effect the saturated magnitudes had on the rescue efforts. Also, there is no simple relation between magnitude and possible destruction, since factors like distance from the event and quality of the buildings have to be considered.

The use of M_S requires large epicentral distances, which means that it normally cannot be used in local networks. To overcome this problem, Singh and Pacheco (1994) developed two magnitude scales for Mexico tied to the seismic moment for automatic implementation, one based on long-period (15–30 sec) amplitudes and an energy-based scale in which an integration of the velocity spectrum is performed. The energy scale is based on a modified relation between energy and M_w and was shown to work up to magnitude 8.

In this article we present a method to automatically determine the moment magnitude for local and regional distances from the source spectrum of *P, S*, or *Lg* waves. The routine is simpler than a moment tensor inversion and can provide a magnitude estimate based on a single station. With data from Mexico, Norway, and the Deception Island regions we attempt to show that M_w can be computed over the entire magnitude range in most seismic environments. All that is needed is some knowledge of the local or regional attenuation.

Source Parameters and Moment Magnitude

The displacement spectral amplitude $A(f)$ after removal of the instrument response, is given by

$$A(f) = S(f)D(f)G(R), \tag{1}$$

where R is the hypocentral distance, $S(f)$ is the source term, $D(f)$ is the diminution function, and $G(R)$ is the geometrical spreading. Equation (1) is valid for both *P* and *S*/*Lg* waves with different $S(f)$, $D(f)$, and $G(R)$ terms for the respective wave types. With the term *P* waves we refer to all primary wave types and with *S*/*Lg* waves we refer to all nonprimary types, including surface waves. The source term for a simple ω^2 model is given by (Aki, 1967; Brune, 1970, 1971)

$$S(f) = \frac{M_0}{4\pi k \rho v^3}\left[1 + \frac{f^2}{f_c^2}\right]^{-1}, \tag{2}$$

where M_0 is the seismic moment, $k = (\sqrt{2.0 \times 0.6})^{-1} = 0.83$ is a factor to correct for free-surface reflection (factor 2) and for the rms average of the displacement radiation pattern (factor 0.6, neglecting the difference between *P*- and *S*-wave radiation pattern), ρ is the density, v is either the *P*- or *S*-wave velocity at the source, and f_c is the corner frequency. For $f < f_c$ the source-amplitude spectrum is flat and proportional to the seismic moment and drops proportional to ω^{-2} for $f > f_c$. Thus M_0 can easily be determined from the long period part of the source spectrum. The diminution function $D(f)$ consists of two parts,

$$D(f) = P(f)N(f). \tag{3}$$

$P(f)$ accounts for losses along the travel path

$$P(f) = \exp\left[\frac{-\pi T f}{Q(f)}\right], \tag{4}$$

where T is the travel time, which for *Lg* and surface waves is given by R/v_g with the hypocentral distance R and the group velocity v_g. $Q(f)$ is the frequency-dependent quality factor, often given in the simple form of (e.g., Aki, 1980)

$$Q(f) = Q_0 f^{\alpha}. \tag{5}$$

The ratio of Q for P (Q_α) and S (Q_β) waves is a function of frequency (Sato and Fehler, 1998). For frequencies below 1 Hz, the ratio Q_β/Q_α is about 0.5, while it is between 1 and 2 for frequencies larger than 1 Hz.

The term $N(F)$ accounts for the near-surface losses

$$N(f) = exp(-\pi\kappa f), \tag{6}$$

where κ depends on the quality factor in the near-surface layers. $N(f)$ is mentioned for completeness, however, the correction for $N(f)$ was not applied in the analysis during this study, since it is not well enough understood for all regions presented here. The correction for $N(f)$ has been discussed for small-sized earthquakes recorded at short distances by Singh et al. (1982), Anderson and Hough (1984), Abercrombie (1997), and Prejean and Ellsworth (2001).

The geometrical spreading for *P* waves is

$$G(R) = \frac{1}{R}, \tag{7}$$

while the geometrical spreading for *S*/*Lg* waves is given by (Herrmann and Kijko, 1983)

$$G(R) = \begin{cases} R^{-1} & f \text{ or } R \le 100 \text{ km} \\ (100 \times R)^{-1/2} & f \text{ or } R \ge 100 \text{ km} \end{cases}. \tag{8}$$

This form of $G(R)$ for *S*/*Lg* waves implies dominance of body waves for $R \le 100$ km and of surface waves for $R \ge 100$ km and assumes shallow focus earthquakes.

The moment magnitude was defined by Kanamori (1977) through the linear relation of energy and magnitude. The M_w scale is given by

$$M_w = \frac{2}{3}\log M_0 - 10.7, \tag{9}$$

where M_0 is given in Nm. In general M_S and M_w are similar for $4 < M_S < 8$ (Ekström and Dziewonski, 1988). For smaller magnitudes (M_S <4) M_w needs to be compared with M_L or M_c. Relations between the seismic moment and other magnitude scales were discussed by Bakun (1984) and Ekström and Dziewonski (1988). The primary goal of this study is to show that the source parameters can be determined automatically. However, we will also show that the M_w obtained compares well with other magnitudes determined.

Method

Data Preparation

The time domain signal of *P* or *S*/*Lg* waves was extracted from the vertical component seismograms, since the vertical component is less affected by soil amplification and generally available on all stations. The time window for extracting the *Lg* waves was defined by a group velocity window through

$$OT + R/v_{g,max} \leq T \leq OT + R/v_{g,min}, \qquad (10)$$

where *OT* is the origin time, *R* is the hypocentral distance, and $v_{g,min/max}$ are the minimum and maximum group velocities considered. The length of the extracted signal duration thus increases with distance. For *P* and *S* waves, either a fixed time window or a time window corresponding to a group velocity range, starting with either the manually picked or computed phase onset was used. Clipped data was disregarded. The data was transformed into the frequency domain using a standard FFT routine. Following equation (1), for a given hypocenter location, the source spectrum was obtained from the amplitude spectrum by removing the effect of attenuation and geometrical spreading. The spectrum was not smoothed. From equation (2) it is seen that the shape of the source spectrum depends on two parameters only, M_0 and f_c.

The main problem when determining these parameters in an automatic procedure is that the real data normally will not follow the ω^2 model over the entire frequency range. The source complexity in large earthquakes and propagation effects can cause deviation. In addition, depending on the earthquake size and distance from the station, the earth noise spectral level may be on the same order as the level of the signal and can dominate the spectral shape at both low and high frequencies. Therefore, it is essential to determine the frequency range over which the observed spectral levels are significantly higher than the noise. To not process noisy traces, the noise spectrum prior to the first phase arrival was computed, and it was required that at some frequency, the signal spectrum be at least 2.5 times the noise spectrum. The lower bound of the frequency range was selected as the frequency from which the difference of signal and noise be at least half of the maximum difference over the complete frequency range. The upper bound of the frequency range was defined by the global minimum in signal spectral amplitude. It was additionally required that the frequency range be large enough ($\log(f_{max}) - \log(f_{min}) > 0.1$) and that the average ratio between signal and noise spectral amplitudes in the selected frequency range be above a threshold value (>1.5). For large events recorded on broadband sensors, normally the entire frequency range can be used, since the noise spectral levels are far below the signal.

Determining M_0 and f_c

The parameters M_0 and f_c were determined by minimizing the difference between the observed and synthetic source spectral amplitudes. The error function *E* that was minimized is of the form

$$E = \left[\sum_i |a_{i,obs} - a_{i,synth}|^n \right]^{1/n}, \qquad (11)$$

where $a_{i,obs}$ and $a_{i,synth}$ are the observed and synthetic spectral amplitudes respectively and *n* is the norm. Here we used $n = 1$, since it was found that $n = 1$ and $n = 2$ produce equally good results. M_w is determined from M_0 (equation 9), as average if more than one observations are available.

To obtain M_0 and f_c we tested two search algorithms: a converging grid search and a standard genetic algorithm (GA) (e.g., Holland, 1975; Michalewicz, 1992). In the converging grid search, the model space is divided into a grid and the error function determined for all grid points. In an iterative procedure, a smaller grid with denser spacing around the best solution is generated and evaluated. The best solution is obtained after a few iterations. The GA starts by randomly building a population of a fixed size and the error function is determined for all individuals in the population. The population is then modified through random crossover between individuals and mutation of individuals. The new generation is formed by evaluating the error function and involves a random selection process. Over the generations, better solutions should become more numerous within the population. The best solution is the one with the smallest error function from all generations. While the grid search is guaranteed to find the global minimum, the GA is likely to find the global minimum, but since it is a random approach it is possible that not the full model space is searched.

Data

The automatic routine for determination of source parameters was tested for three very different seismic environments (Fig. 1):

1. *Mexico*. Mexico is regularly affected by large and often damaging, mostly shallow earthquakes located in the subduction zone along the coast (Singh and Ordaz, 1994). The Mexican data was recorded on broadband stations

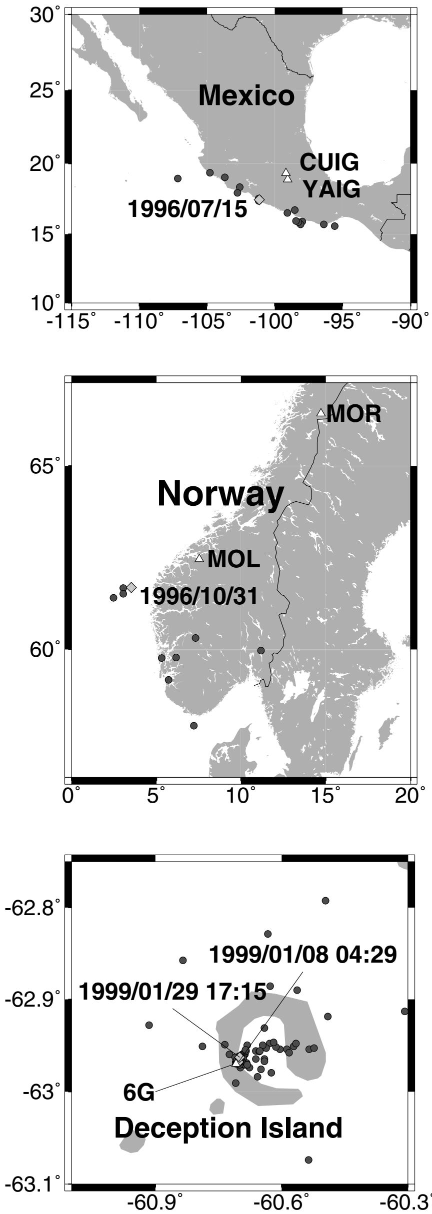

Figure 1. Epicenter maps (Mercator projection) for the data sets used in this study. Northern latitudes and eastern longitudes are positive. The events of Figures 2–4 are plotted as diamonds and labelled; the station locations are indicated by triangles.

operated by the National Seismological Service (SSN), at the National Autonomous University of Mexico (Pacheco, 2002). The selected data set consisted of 16 events with a total of 127 observations. The hypocentral distances were within 30–1730 km and the magnitudes in the range 4.2–7.6 (Table 1, M_w, this study). The selected earthquakes were all shallow with a maximum depth of 40 km.

2. *Norway*. Earthquakes occurring in Norway are crustal and mostly of small to moderate size (Bungum *et al.*, 1991). The data were recorded on short-period and broadband seismic stations that are part of the Norwegian National Seismic Network (NNSN), which is operated by the University of Bergen (Atakan and Havskov, 2002). A total of 64 recordings from 10 crustal earthquakes, with distances of 30–1330 km, in the magnitude range 2.0–4.2 (Table 2, M_w this study) were used.
3. *Deception Island*. The Andalusian Institute of Geophysics, University of Granada, operates a short-period seismic array on the Antarctic Deception Island (Saccorotti *et al.*, 2001; Ibañez *et al.*, 2002). In the period 1994–1998, mostly volcanic events related to the water–magma interaction and only few tectonic events were observed. This changed in the first three months of 1999, when more than 3000 volcano-tectonic events were recorded (Havskov *et al.*, 2002). The data used in this study was recorded in the time period January to February 1999 and consisted of 151 volcano-tectonic events in the magnitude range -1.1–2.1 (M_w, this study). In the analysis, only one station representative for the array was processed. The hypocentral distance range was up to 22 km.

The hypocenter locations of the events were taken from the bulletins of the respective institutions. For the data sets from Mexico and Norway, the time window was computed based on location and origin time, while for the Deception Island manual phase picks were used to define the time window. The spectral analysis was first performed for the *S*/*Lg* waves manually using the SEISAN analysis software (Havskov and Ottemöller, 2000). The manual analysis was done on the same time window as used in the automatic processing. The spectra were approximated by two lines corresponding to the flat level at low frequencies and the decay for frequencies larger than f_c, which can differ from the ω^2 decay. The quality factors and group velocity or fixed time windows used are given in Table 3. For Mexico and Deception Island, the same Q for P and *S*/*Lg* waves was used. For Norway, Q for P was selected so that the obtained spectral levels were the same as from *Lg* waves.

Examples of typical source spectra for Mexico, Norway, and Deception Island are shown in Figures 2, 3, and 4, respectively. The frequency range over which the observed spectrum is matched depends on the earthquake size. The frequency range shifts from low frequencies (0.01–10 Hz) for the moderate to large earthquakes in Mexico to higher frequencies (0.1–20 Hz) for the small to moderate size events in Norway, and even higher frequencies (1.0–> 100 Hz) for the events from Deception Island. The frequency range was selected automatically through comparison with the noise spectrum as described in the previous section.

Results and Discussion

The two methods, converging grid search and genetic algorithm, were tested for their cost-effectiveness when applied to the three data sets (Fig. 5). The converging grid search was found to be significantly more cost-effective.

Table 1

Parameters of Mexican Earthquakes

Date yyyy/mm/dd	Time (GMT)	Lat. °N	Lon. °E	Depth in km	Harvard* M_w	M_A†	M_E†	Manual‡ $M_w(Lg)$	Auto‡ M_w (Lg)	Auto‡ $M_w(P)$	*n* Stations
1995/09/14	1404	16.730	−98.540	21.8	7.3	6.7	7.0	7.0	6.9	6.7	3
1995/10/09	1536	19.340	−104.800	15.0	8.0	7.0	7.6	7.6	7.3	7.1	4
1995/10/12	1653	19.040	−103.700	11.0	5.9	5.9	6.2	6.0	6.0	5.8	5
1996/02/25	0308	15.880	−97.980	15.0	7.1	—	—	6.9	6.8	6.4	4
1996/03/13	2104	16.520	−99.080	18.0	5.1	5.1	5.3	5.1	5.1	5.0	5
1996/06/10	0853	15.670	−98.130	25.0		—	—	4.2	4.5	4.0	4
1996/07/15	2123	17.450	−101.160	20.0	6.6	6.4	6.4	6.5	6.5	6.6	6
1996/07/16	1139	17.360	−101.220	10.0		4.7	4.8	4.5	4.7	4.4	7
1996/07/18	0816	17.540	−101.200	20.0	5.4	4.7	4.7	5.0	5.1	4.9	5
1997/01/11	2028	18.340	−102.580	40.0	7.1	6.7	7.3	6.9	7.0	6.5	10
1997/01/16	2141	17.940	−102.760	25.0	5.5	5.3	5.4	5.5	5.5	5.2	11
1997/05/01	1137	18.960	−107.150	15.0	6.9	6.1	6.3	7.3	7.4	6.9	4
1997/07/19	1422	15.860	−98.260	15.0	6.7	6.3	6.4	6.6	6.7	6.4	8
1997/08/25	0515	15.950	−98.430	5.0		4.7	4.2	4.6	4.5	4.4	8
1998/02/03	0302	15.690	−96.370	33.0	6.3	6.2	6.5	6.4	6.4	6.3	12
1998/11/07	1229	15.550	−95.580	7.0		4.9	5.1	4.9	4.9	5.0	11

*from the Harvard CMT catalog
†computed by the SSN Mexico
‡this study

Table 2

Parameters of Norwegian Earthquakes

Date yyyy/mm/dd	Time (GMT)	Lat. °N	Lon. °E	Depth in km	Manual M_L*	Manual M_w (Lg)	Auto M_w (Lg)	Auto M_w (P)	*n* Stations Used
1995/07/29	0023	60.345	7.319	5.0	1.7	2.0	2.0	1.9	7
1995/08/13	0959	61.502	2.460	15.0	2.4	2.4	2.5	2.4	7
1995/11/13	0122	59.975	11.172	14.0	3.0	3.1	3.1	2.8	8
1995/12/03	0453	59.764	6.169	15.0	2.3	2.2	2.2	2.0	5
1996/06/25	0337	61.763	3.040	17.0	3.2	3.4	3.4	3.4	6
1996/10/31	1252	61.790	3.533	20.0	3.7	3.6	3.7	3.5	9
1999/02/06	2327	61.606	3.063	13.0	2.1	2.3	2.4	2.4	5
2000/08/12	1427	59.748	5.329	18.0	4.4	4.1	4.2	4.3	7
2000/09/01	1148	59.101	5.737	25.0	2.6	2.8	2.7	2.9	7
2000/10/19	1027	57.666	7.213	7.0	3.3	3.2	3.3	3.2	9

*using the M_L scale by Alsaker *et al.* (1991)

Table 3

Quality Factor and Group Velocities or Absolute Time Window Length

			Group Velocities (km/sec)		Fixed Time (sec)	
Region	$Q(f)$	Reference for $Q(f)$	*P*	*Lg*	*P*	*S*
Mexico	$204f^{0.85}$	Ottemöller *et al.*, 2001	5.0–6.5	2.0–3.7	—	—
Norway	$Q_{S/Lg}(f) = 470 f^{0.7}$ $Q_P(f) = 600f^{0.7}$	Kvamme *et al.*, 1995 this study	5.0–6.5	3.0–3.7	—	—
Deception Island	$58f^{0.40}$	Havskov *et al.*, 2002	—	—	0.2	3.0

However, the computation time needed to obtain the best fit is about the same for both methods. Therefore, all results presented here were obtained with the converging grid search.

For the Mexican data set, the automatically determined magnitudes only showed minor differences from the manually determined values. The maximum difference seen was ΔM_w 0.3 (Table 1). While M_w computed here was generally close to the Harvard M_w, the maximum difference ΔM 0.7 was quite significant (Table 1). The automatic M_w values also compare reasonably well with the M_E and M_A determined by the Mexican SSN (Table 1). However, for the event on 1 May 1997, there is a significant variation between the scales, Harvard M_w 6.9, M_E 6.3, and $M_{w,Lg,auto}$ 7.4. It seems

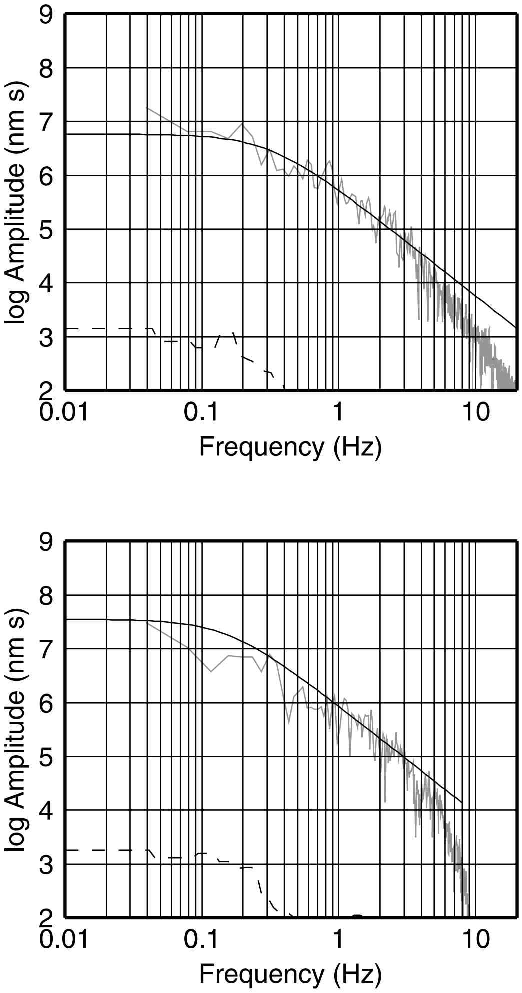

Figure 2. Typical source spectra obtained from broadband sensors, YAIG (top, $\Delta = 271$ km) and CUIG (bottom, $\Delta = 295$ km), for the M_w 6.6 event of 15 July 1996 (Table 1) recorded in Mexico. The location of the event is shown in Figure 1. The grey lines show the observed source spectra; the black solid lines show the theoretical spectra based on the results from the automatic procedure (note that the theoretical spectra are only shown for the frequency range used in the automatic routine); and the dashed lines show the noise spectra, taken from the signal before the first phase arrival.

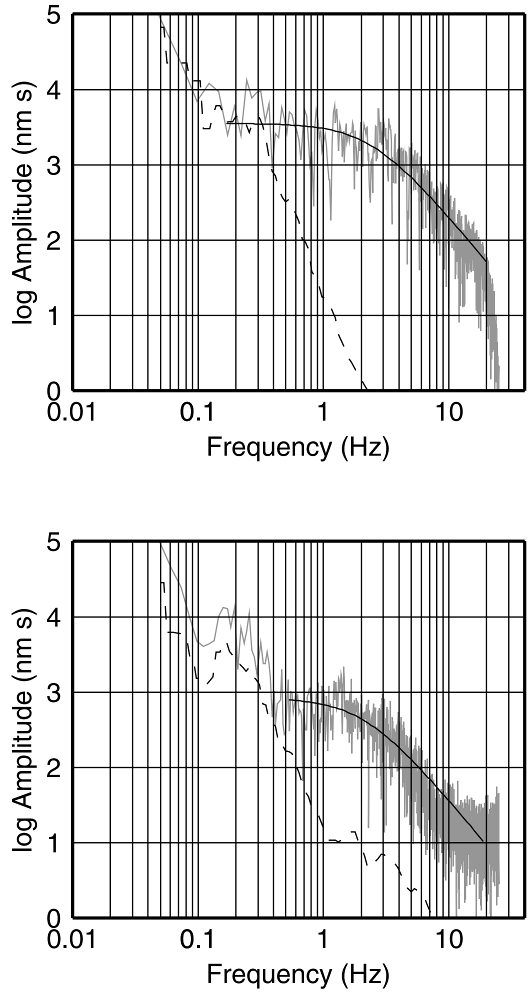

Figure 3. Typical source spectra obtained from short-period sensors, MOL (top, $\Delta = 226$ km) and MOR (bottom, $\Delta = 740$ km), for the M_L 3.7 event of 31 October 1996 (Table 2) recorded in Norway. The location of the event is shown in Figure 1. For explanation, see the Figure 2 caption.

that while the automatic routine works consistently well, measured through comparison with manual analysis of the same data, the variation of the various scales changes between events, possibly due to the different source parameters.

For earthquakes with $M > 7$ the moment magnitudes determined from the source spectra seem to be slightly lower than the values reported in the Harvard CMT catalog. Unlike for other magnitude scales, this cannot be explained by saturation related to measuring at too high frequencies, since the entire frequency range is used. It is possible though that for large earthquakes recorded on stations close to the epicenter, the time window is too short to measure the spectral amplitudes at frequencies below the corner frequency, since the lowest frequency value in the FFT is the inverse of the signal duration in the time domain. This can be a problem, in particular, with *P* waves since the duration in time is limited by the arrival of the *S* waves. For example, at a distance of 500 km, the *P–S* time would be about 50 sec. The differences as compared with Harvard could possibly reflect uncertainties in the Harvard catalog as well as uncertainties in our method. For Mexican earthquakes, Singh and Pacheco (1994) discussed the possibility of the Harvard catalog overestimating the moment due to a too high depth estimate.

For the Norwegian data set, a good match of automatically and manually determined M_w and f_c was found (Table 2, Fig. 7). The maximum difference between manually and automatically determined $M_{w,Lg}$ was 0.1. Also, the M_w values were found to be similar (ΔM_{max} 0.3) to the M_L values re-

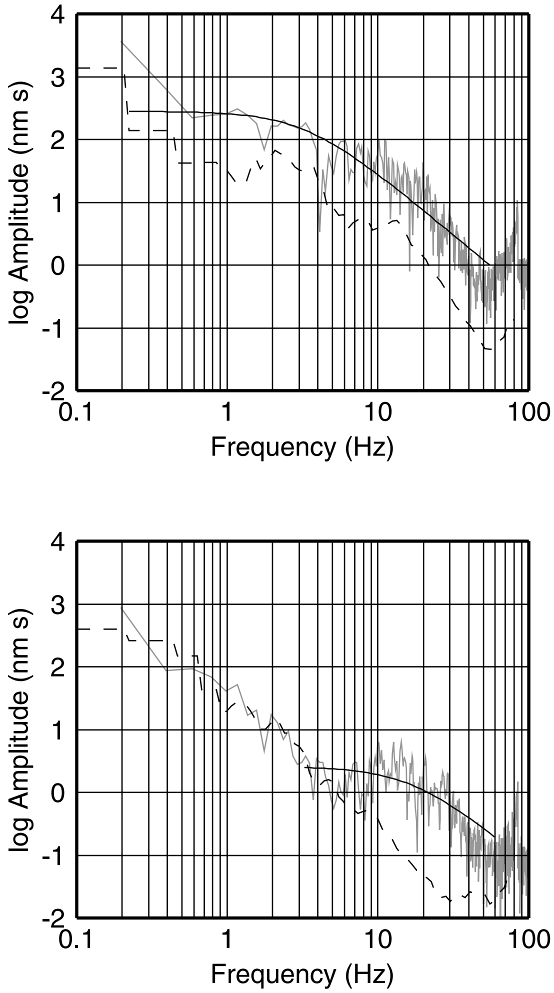

Figure 4. Typical source spectra obtained from the station 6G on Deception Island. The figures are from a M_w 0.8 (top, $\Delta = 0.97$ km) on 29 January 1999 and M_w -0.7 event (bottom, $\Delta = 0.42$ km) on 8 January 1999. The locations of the events are shown in Figure 1. For explanation, see the Figure 2 caption.

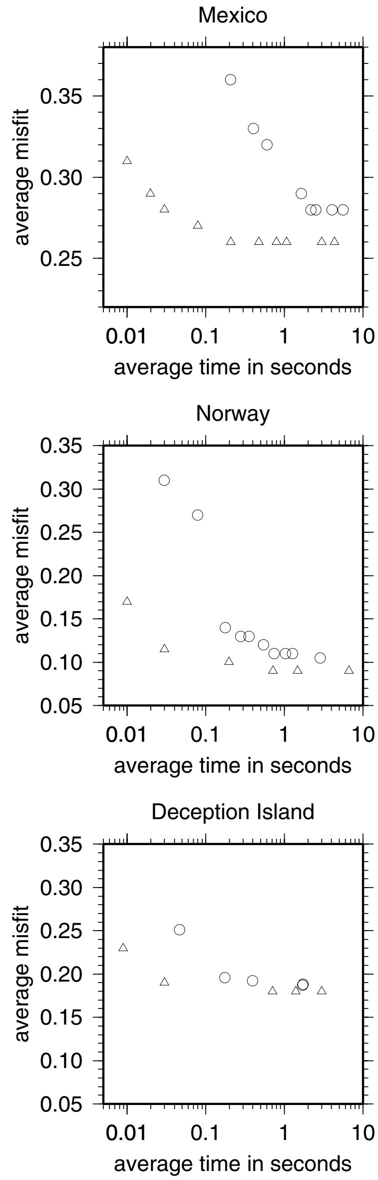

Figure 5. Comparison of cost-effectiveness between the converging grid-search (triangle) and the genetic algorithm (circles). The misfit (equation 11) averaged over all observations is plotted against the required computation time (on a 700-Mhz Pentium III).

ported by the NNSN based on the scale by Alsaker *et al.* (1991).

Application of the method to the Deception Island data set (Fig. 8) showed that there is practically no lower magnitude limit to determine the seismic moment from the source spectrum in an automated procedure (Hanks, 1982). It is seen that the automatic moment values are slightly higher than the manually determined ones. This is possibly explained by assuming an ω^2 model in the automatic routine, while the decay can be of higher order in the manual analysis. The M_w values were comparable to the M_L values (Fig. 10), see Havskov *et al.* (2002) for a detailed discussion. Thus, the procedure described here can be used to automatically determine M_w from small earthquakes as they occur in large numbers in volcanic environments, as aftershocks or swarms. Due to the large number of events, manual analysis in these situations is often not feasible.

For the three data sets, it was found that both automatic routines to determine the seismic moment from both *P*- and *S*/*Lg*-wave source spectra produced results close to the manual analysis. The maximum difference observed was ΔM_{max} 0.3 while the computed error was $\Delta M \pm 0.5$ (Figs. 6 and 7). The automatically determined corner frequencies, however, showed significant variation from the manually determined values. The main focus here is towards automatic magnitude determination, which does not seem to be affected by the possible variability in f_c determination.

Although there is no lower magnitude limit for this

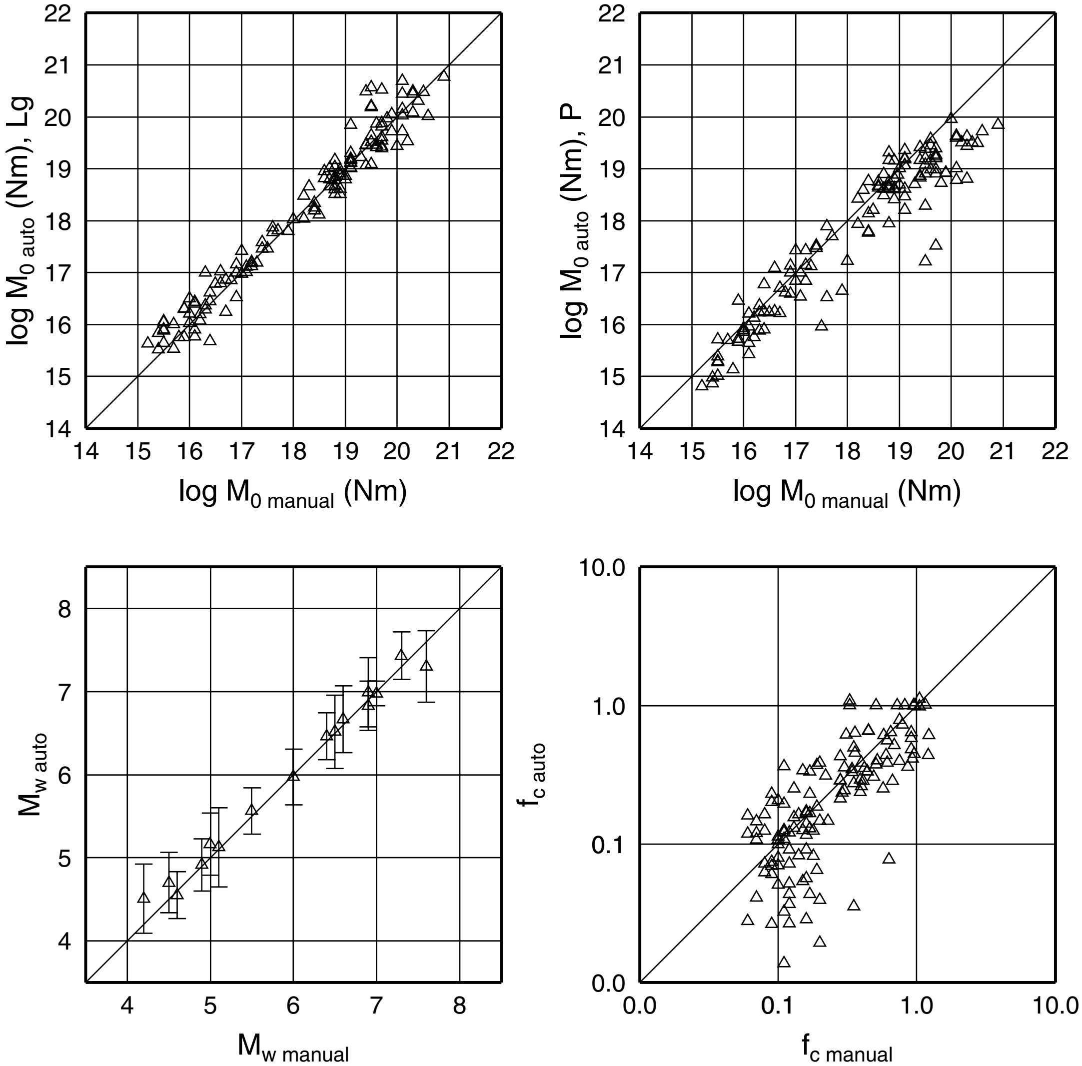

Figure 6. Comparison of automated and manual analysis for the Mexican data set. The comparison of seismic moment is shown for both *Lg*-and *P*-wave spectra. The M_w auto values are averages from *Lg*-wave spectra based on several measurements for each event. The error bars for M_w represent one standard deviation.

method (Hanks, 1982), the signal needs to be significantly higher than the noise amplitudes, where the ratio of signal and noise depends on both the earthquake size and the hypocentral distance. In addition, the corner frequency for small events could be higher than the recording system's Nyquist frequency. The difference in the determination of f_c between manual and automatic processing can be explained by the use of the ω^2 source in the automatic routine, while there is no constraint on the decay rate in the manual processing. Also, in order to obtain correct corner frequencies, the near-surface attenuation needs to be considered. Without correction for $N(f)$, the decay at high frequencies appears steeper than predicted by the ω^2 model. This will result in systematically underestimated f_c compared with the manual analysis, as seen with the Deception Island data (Havskov *et al.*, 2002).

The differences for the seismic moment obtained from *P* and *S*/*Lg* waves are minor (Fig. 9); however, toward larger magnitudes ($M_w > 6.4$) the M_w values obtained from *P* waves tend to be below the values derived from *Lg* waves (Table 1). This is possibly explained by the shorter duration of *P* waves compared with *S* waves as mentioned above. It is possible that the difference in the determination of seismic moment from *P* and *S*/*Lg* wave could be further reduced by a better knowledge of *Q*. While in general, the use of *Lg* waves would be preferable, the additional analysis of *P*-wave spectra gives additional observations and thus may provide a more reliable average estimate, for example by reducing the radiation pattern effect. For deeper events and oceanic travel paths the analysis has to be based on *P* waves, since *Lg* waves may not be generated or may be blocked in transition zones between oceanic and continental crust. The

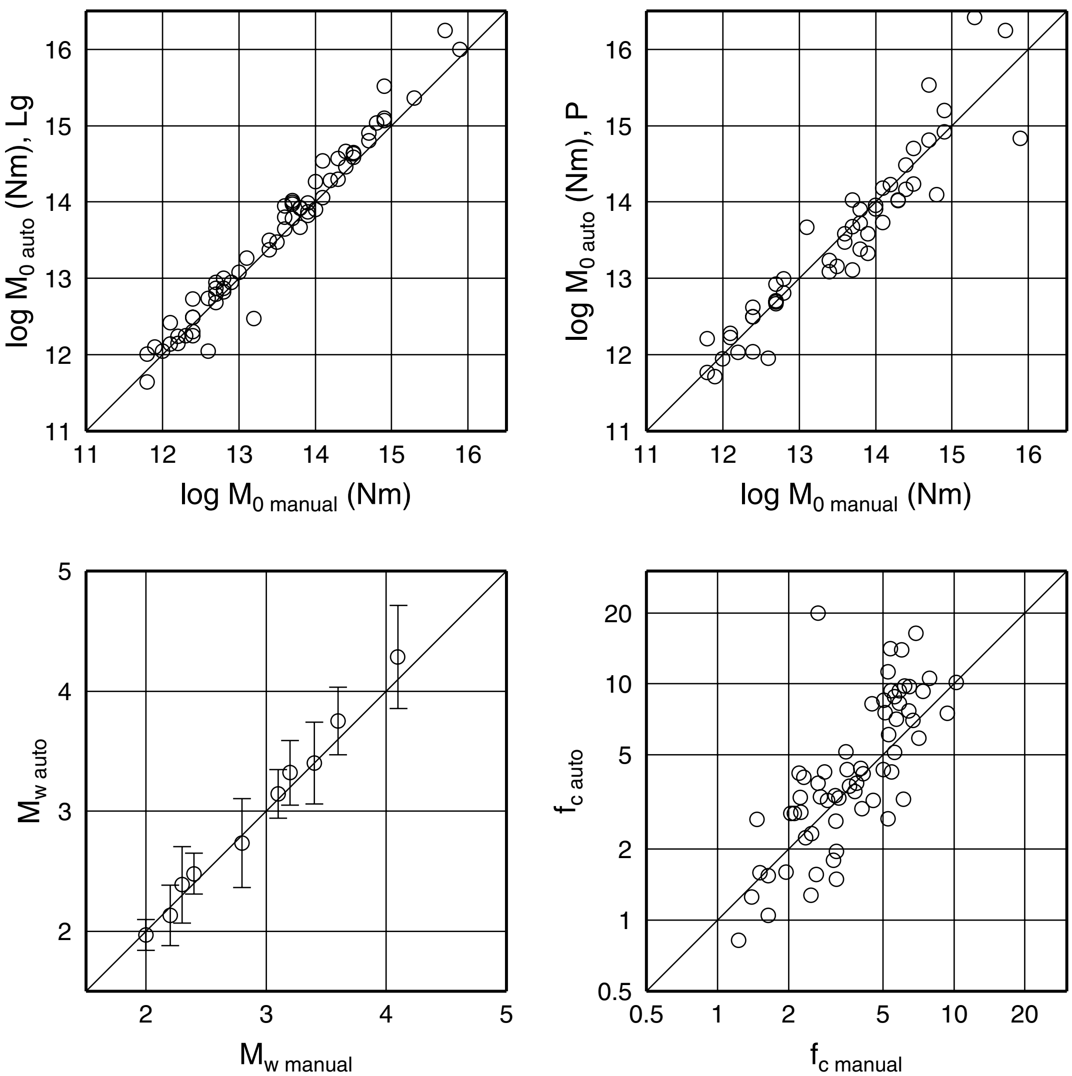

Figure 7. Comparison of automated and manual analysis for the Norwegian data set. The comparison of seismic moment is shown for both *Lg*- and *P*-wave spectra. The M_w auto values are averages from *Lg*-wave spectra based on several measurements for each event. The error bars for M_w represent one standard deviation.

use of *P*-wave data can be of particular interest when the *S*/*Lg*-wave data is clipped or in a situation where the rapid determination is the main goal, obviously *P* waves have the advantage of arriving earlier than *S*/*Lg*.

To provide wider use of M_w from *P*- and *S*/*Lg*-wave spectra, it is important to compare the estimates to other magnitude scales in use (Figure 10). The M_w estimates for the Mexican events were compared to the Mexican energy scale M_E, since M_A is saturated for large events (Singh and Pacheco, 1994). The M_w estimates for the earthquakes from Norway and Deception Island were compared with the local magnitudes (M_L). It was seen that there is a good correspondence between M_w and the other scales. This indicates that M_w is not only valid for the entire magnitude range, but also provides estimates comparable to traditionally used scales. However, this needs to be further investigated with a large data set from additional regions.

Moment magnitudes are routinely determined through automatic regional moment tensor inversion where, at present in the best case, results can be obtained within 10 min after earthquake occurrence (e.g., Kawakatsu, 1995; Pasyanos *et al.*, 1996). However, the automatic moment tensor inversion is not yet feasible in many seismic networks due to low station density and the widespread use of short-period sensors. In addition, the computation of Green's functions for small events is more difficult, which means that the moment tensor inversion is more problematic for small events (M_w <4). However, while the moment tensor inversion fully accounts for the radiation pattern, the radiation pattern is averaged out and thus basically ignored in the approach presented here. The method presented here could be an attractive alternative in many networks, since the routine is simple, fast, reliable, and works for the smallest earthquakes. Theoretically, a minimum of only one station is required,

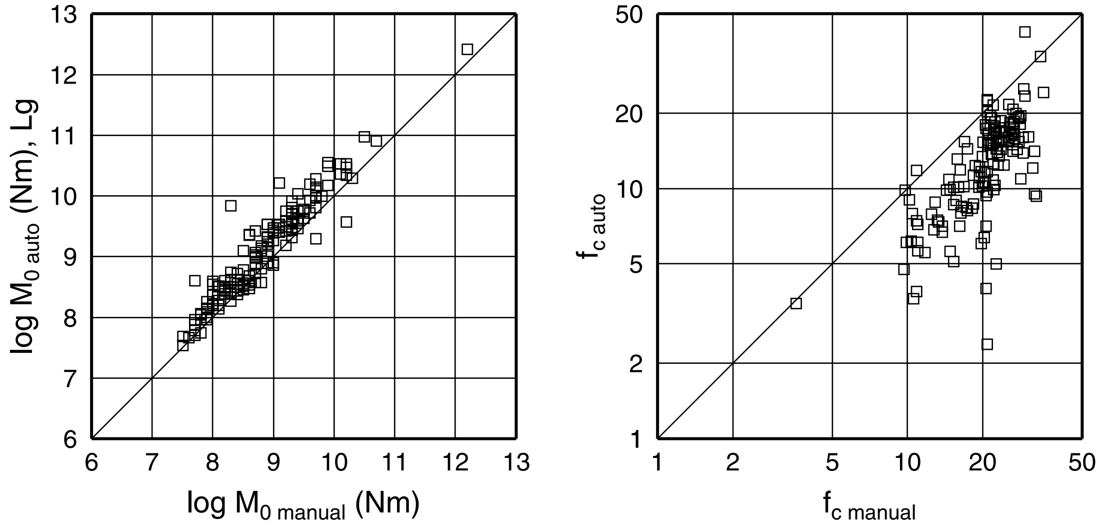

Figure 8. Automatically determined M_w and f_c for the Deception Island data set based on the *Lg*-wave spectrum versus the manually determined parameters. The values were determined from a single station.

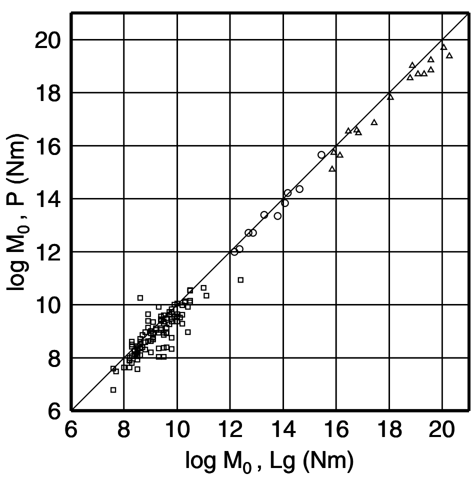

Figure 9. Comparison of the average seismic moment determined for single events from *P*- and *S*/*Lg*-source spectra, respectively. The three data sets shown are Mexico (triangle), Norway (circle), and Deception Island (square).

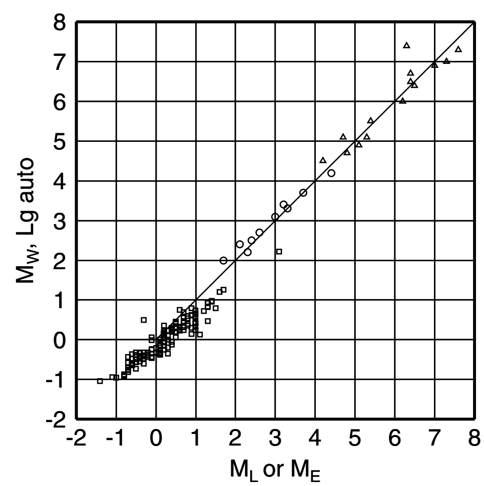

Figure 10. Comparison of the automatically determined average M_w from *S*/*Lg* waves with other magnitude scales. The comparison is with M_E for Mexico (triangle), with M_L for Norway (circle) and with M_L for the Deception Island (square).

however, in this case the result would reflect the radiation pattern. The implementation of automatic moment magnitude determination into automatic processing systems in the case of large earthquakes would, most importantly, provide an unsaturated measure of the earthquake size.

Conclusions

An automatic procedure to determine M_w for earthquakes recorded at local and regional distances using simple amplitude spectra was developed and tested with three data sets. The main conclusions are:

- Due to its application over a wide magnitude range ($-1 < M < 8$) without saturation for great earthquakes and being comparable to other common magnitude scales, the moment magnitude scale should become more widespread.
- The two automated algorithms to determine the seismic moment from both *P*- and *S*/*Lg*-source spectrum produced results close to the manual analysis. The converging grid-search was more cost-effective than the GA. The determination of f_c is less reliable.
- The automated algorithm to determine M_w is faster than a full source inversion. For large and shallow earthquakes

(M >6.5), the *Lg*-source spectrum has to be used, since the *P*-wave duration may be too short to reflect the high energy carried at long periods.
- The use of an automatic routine to determine source parameters makes the analysis of large data sets of small to moderate earthquakes feasible.

Considering the simplicity of the procedure, the reliability of the estimate and the need for a magnitude scale that is based on a physical quantity, these results should give a good argument for the more widespread use of the automatic and manual determination of M_w.

Acknowledgments

We would like to thank the National Seismological Service at the National Autonomous University of Mexico, the Andalusian Institute of Geophysics, University of Granada, and the Norwegian National Seismic Network operated by the University of Bergen for providing the data. The M_E and M_A values for Mexico were kindly computed by Arturo Iglesias. We appreciate the discussions with S. K. Singh on the Mexican earthquakes. Comments on the manuscript by Anibal Ojeda are appreciated. The comments by the editor and two anonymous reviewers helped to improve the manuscript. The data from the Deception Island was obtained through the project CYCYT-ANT98-111 under the Spanish Antarctic Research Program. The figures were generated with GMT (Wessel and Smith, 1995).

The computer source code used to implement the method is part of the SEISAN earthquake analysis software, which is freely available from http://www.ifjf.uib/seismo/software/software.html.

References

Abercrombie, R. E. (1997). Near-surface attenuation and site effects from comparison of surface and deep borehole recordings, *Bull. Seism. Soc. Am.* **87,** 731–744.

Al-Eqabi, G. I., K. D. Koper, and M. E. Wysession (2001). Source characterization of Nevada test site explosions and western U.S. earthquakes using *Lg* waves: implications for regional source discrimination, *Bull. Seism. Soc. Am.* **91,** 140–153.

Alsaker, A., L. B. Kvamme, R. A. Hansen, A. Dahle, and H. Bungum (1991). The M_L scale in Norway, *Bull. Seism. Soc. Am.* **81,** 379–398.

Anderson, J. G., and S. E. Hough (1984). A model for the shape of the fourier amplitude spectrum of acceleration at high frequencies, *Bull. Seism. Soc. Am.* **74,** 1969–1993.

Anderson, J. G., and J. R. Humphrey (1991). A least squares method for objective determination of earthquake source parameters, *Seism. Res. Lett.* **62,** 201–209.

Aki, K. (1967). Scaling law of seismic spectrum, *J. Geophys. Res.* **72,** 1217–1231.

Aki, K. (1980). Attenuation of shear-waves in the lithosphere for frequencies from 0.05 to 25 Hz, *Phys. Earth Planet. Interior* **21,** 50–60.

Atakan, K., and J. Havskov (2002). The Norwegian National Seismic Network (NNSN), *Scandinavian Oil and Gas Magazine* **7,** 28–32.

Bakun, W. H. (1984). Seismic moments, local magnitudes, and coda-duration magnitudes for earthquakes in central California, *Bull. Seism. Soc. Am.* **74,** 439–458.

Brune, J. N. (1970). Tectonic stress and the spectra of seismic shear waves from earthquakes, *J. Geophys. Res.* **75,** 4997–5009.

Brune, J. N. (1971). Correction, *J. Geophys. Res.* **76,** 5002.

Bungum, H., A. Alsaker, L. B. Kvamme, and R. A. Hansen (1991). Seismicity and seismotectonics of Norway and nearby continental shelf areas. *J. Geophys. Res.* **96,** 2249–2265.

Ekström, G., and A. M. Dziewonski (1988). Evidence of bias in estimations of earthquake size, *Nature* **332,** 319–323.

Espinosa Aranda, J. M., A. Jiménez, G. Ibarrola, F. Alcantar, A. Aguilar, M. Inostroza, and S. Maldonado (1995). Mexico City seismic alert system, *Seism. Res. Lett.* **66,** 42–53.

Gee, L. S., D. S. Neuhauser, D. S. Dreger, M. E. Pasyanos, R. A. Urhammer, and B. Romanowicz (1996). Real-time seismology at U.C. Berkeley: The rapid earthquake data integration project, *Bull. Seism. Soc. Am.* **86,** 936–945.

Grant, J. A., and L. Mansinha (1977). Seismic magnitude from fourier analysis, *Bull. Seism. Soc. Am.* **67,** 453–461.

Gupta, H. K., N. P. Rao, B. K. Rastogi, and D. Sarkar (2001). The deadliest intraplate earthquake, *Science* **291,** 2101–2102.

Hanks, T. C., and H. Kanamori (1979). A moment magnitude scale, *J. Geophys. Res.* **84,** 2348–2350.

Hanks, T. C. (1982). f_{max}, *Bull. Seism. Soc. Am.* **72,** 1867–1879.

Havskov, J., and L. Ottemöller (2000). SEISAN: The earthquake analysis software, Version 7.1, University of Bergen, Bergen, Norway, 236 pp.

Havskov, J., J. A. Peña, J. M. Ibáñez, L. Ottemöller, and C. Martínez-Arévalo (2002). Magnitude scales for very local earthquakes. Application for deception island volcano (Antarctica), *J. Volcan. Geotherm. Res.* (in press).

Herrmann, R. B., and A. Kijko (1983). Modelling some empirical vertical component Lg relations, *Bull. Seism. Soc. Am.* **73,** 157–171.

Holland, J. H. (1975). *Adaption in Natural and Artificial System*, University of Michigan Press, Ann Arbor, Michigan.

Ibañez, J. M., E. Carmona, J. Almendros, G. Saccorotti, E. Del Pezo, M. Abril, and R. Ortiz (2002). The 1998–1999 seismic series at Deception Island volcano, Antarctica. *J. Volcan. Geotherm. Res.* (in press).

Johnson, C. E., A. Bittenbinder, B. Bogaert, L. Dietz, and W. Kohler (1995). EARTHWORM: a flexible approach to seismic network processing, *IRIS Newsletter XIV* **2,** 1–4.

Kanamori, H. (1977). The energy release in great earthquakes, *J. Geophys. Res.* **82,** 1981–1987.

Kanamori, H. (1983). Magnitude scale and quantification of earthquakes, *Tectonophysics* **93,** 185–199.

Kawakatsu, H. (1995), Automated near-realtime CMT inversion, *Geophys. Res. Lett.* **22,** 2569–2671.

Kvamme, L. B., R. A. Hansen, and H. Bungum (1995). Seismic-source and wave-propagation effects of Lg waves in Scandinavia, *Geophys. J. Int.* **120,** 525–536.

Lomnitz, C., and S. R. Eliarrarás (2001). El Salvador 2001: earthquake disaster and disaster prevention preparedness in a tropical volcanic environment, *Seism. Res. Lett.* **72,** 346–351.

Malone, S. (1996). "Near" realtime seismology, *Seism. Res. Lett.* **67,** 52–54.

McEvilly, T. V., and E. L. Majer (1982). ASP: an automated seismic processor for microearthquake networks, *Bull. Seism. Soc. Am.* **72,** 303–325.

Michalewicz, Z. (1992). *Genetic Algorithms + Data Structures = Evolution programs*, Springer, New York.

Miyamura, S. (1982). On the importance of continuity of magnitude scales, *Tectonophysics* **84,** 47–55.

Nortmann, R., and S. J. Duda (1983). Determination of spectral properties of earthquakes from their magnitudes, *Tectonophysics* **93,** 251–275.

Ottemöller, L., N. M. Shapiro, S. K. Singh, and J. F. Pacheco (2002). Lateral variation of Lg wave propagation in Southern Mexico, *J. Geophys. Res.* **107,** B1.

Pacheco, J. F. (2002). The National Seismological Service of Mexico, In: *International Handbook of Earthquake and Engineering Seismology*, W. H. K. Lee, H. Kanamori, P. C. Jennings, and C. Kisslinger (Editors), Academic Press San Diego (in press).

Pasyanos, M. E., D. S. Dreger, and B. Romanowicz (1996). Toward real-time estimation of regional moment tensors, *Bull. Seism. Soc. Am.* **86,** 1255–1269.

Prejean, S. G., and W. L. Ellsworth (2001). Observations of earthquake source parameters at 2 km depth in the Long Valley caldera, Eastern California, *Bull. Seism. Soc. Am.* **91,** 165–177.

Saccorotti, G, J. Almendros, E. Carmona, J. M. Ibañez, and E. Del Pezzzo (2001). Slowness anomalies from two dense seismic arrays at Deception Island volcano, Antarctica, *Bull. Seism. Soc. Am.* **91,** 561–571.

Sato, H., and M. C. Fehler (1998). Seismic wave propagation and scattering in the heterogeneous earth, Springer, New York.

Schindelé, F., D. Reymond, and E. A. Okal (1995). Analysis and automatic processing in near-field of eight 1992–1994 tsunamigenic earthquakes: Improvements towards real-time tsunami warning, *Pageoph* **144,** 381–408.

Singh, S. K., R. J. Apsel, J. Fried, and J. N. Brune (1982). Spectral attenuation of SH-waves along the Imperial fault, *Bull. Seism. Soc. Am.* **72,** 2003–2016.

Singh, S. K., and J. Pacheco (1994). Magnitude determination of Mexican earthquakes, *Geofís. Int.* **33,** 189–198.

Singh, S. K., and M. Ordaz (1994). Seismic energy release in Mexican subduction zone earthquakes, *Bull. Seism. Soc. Am.* **84,** 1533–1550.

Tajima, F., C. Méngin, D. S. Dreger, and B. Romanowicz (2002). Feasibility of real-time broadband waveform inversion for simultaneous moment tensor and centroid location determination, *Bull. Seism. Soc. Am.* **92,** 739–750.

Toksöz, M. N., R. E. Reilinger, C. G. Doll, A. A. Barka, and N. Yalcin (1999). Izmit (Turkey) earthquake of 17 August 1999: first report, *Seism. Res. Lett.* **70,** 669–679.

Wessel, P., and W. H. F. Smith (1995). New version of the Generic mapping tools released, EOS Trans. Am. *Geophys. Union* **76,** 329.

Withers, M., R. Aster, C. Young, J. Beiriger, M. Harris, S. Moore, and J. Trujillo (1998). A comparison of select trigger algorithms for automated seismic phase and event detection, *Bull. Seism. Soc. Am.* **88,** 95–106.

Wu, Y., T. Shin, C. Chen, Y. Tsai, W. H. K. Lee and T. L. Teng (1997). Taiwan rapid earthquake information release system, *Seism. Res. Lett.* **68,** 931–943.

Institute of Solid Earth Physics
University of Bergen
Allegt. 41
5007 Bergen, Norway
(L.O., J.H.)

Manuscript received 27 July 2001.